Pergamon

Journal of Structural Geology, Vol. 17, No. 5, pp. 677 to 688, 1995

0191-8141/95 $9.50+0.00

0191-8141(94)00092-1

Calcite textures, microstructures and rheological properties of marble mylonites in the Bancroft shear zone, Ontario, Canada

JAY P. BUSCH and BEN A. VAN DER PLUIJM

Department of Geological Sciences, University of Michigan, 1006 C. C. Little Building, Ann Arbor, MI 48109, U.S.A.

(*Received* 31 *January* 1994; *accepted in revised form* 8 *August* 1994)

Abstract—Calcite textures in several microstructural domains from the Bancroft shear zone reveal a sequence of transitions which indicate contributions from a variety of deformation mechanisms at greenschist facies conditions. The coarse marble protolith has undergone low strains accommodated by twinning and grain boundary migration. Porphyroclastic mylonite has a well developed crystallographic preferred orientation and microstructures indicative of dislocation creep and rotation recrystallization mechanisms. The textures are consistent with high-temperature deformation experiments where *r*, *f* and *c* slip systems were active. Complete dynamic recrystallization produced equant, medium-sized grains (50 μm) with a texture that is nearly random. Secondary calcite growth observed under cathodoluminescence and variation in $\delta^{18}O$ value with microstructure indicate large fluid fluxes during mylonitization. Fluid-assisted grain-boundary sliding and a minor component of dislocation creep are the inferred deformation mechanisms. Finer grained *S*–*C* mylonite has a well developed shape fabric and crystallographic preferred orientation with a point maximum and great-circle girdle attributed to attainment of an 'easy slip' orientation for most grains. Ultramylonites have homogeneous textures with fine, elongate grains (20–30 μm) mantled by disseminated secondary phases. Textures in ultramylonites are characterized by single point maxima and great circle girdles. The most evolved ultramylonite has a point maximum oblique to the shear plane with a symmetry indicating rotation of the maximum toward the extension direction.

Texture/microstructure relations in these mylonites indicate that the competition between deformation mechanisms was highly sensitive to grain size, strain and secondary phases in addition to temperature, strain rate and differential stress. The varied deformation mechanisms and application of experimentally-derived constitutive equations indicate significant differences in differential stress and strain rate among microstructural domains. These differences reflect strain softening associated with dynamic recrystallization and work hardening associated with dissemination of secondary phases and the transition from grain-boundary sliding to dislocation creep.

INTRODUCTION

Calcite textures and microstructures in deformed marbles may provide information regarding shear zone kinematics, stress and strain characteristics, and deformation mechanisms. For example, fabric asymmetry relative to the mesostructural framework (foliation and lineation) may yield a criterion for the sense of shear (Schmid *et al.* 1987, Wenk *et al.* 1987). The degree of fabric asymmetry in calcite mylonites has been attributed to the relative contributions of coaxial and non-coaxial strains (Wenk *et al.* 1987, Ratschbacher *et al.* 1991, Erskine *et al.* 1993). Twin density and orientation, subgrain size, recrystallized grain size and dislocation density may be quantitatively related to differential stress magnitudes, orientations and strain (Turner & Weiss 1963, Goetze & Kohlstedt 1977, Schmid *et al.* 1980, Dietrich & Song 1984, Groshong *et al.* 1984). Much of what has been interpreted from naturally deformed calcite rocks and their geological significance is based on numerous deformation experiments and numerical modelling studies (Turner *et al.* 1954, Rutter 1974, Friedman & Higgs 1976, Schmid *et al.* 1977, Schmid *et al.* 1980, Wagner *et al.* 1982, Kern & Wenk 1983, Wenk *et al.* 1986, Schmid *et al.* 1987, Wenk *et al.* 1987, Walker *et al.* 1990, Ratschbacher *et al.* 1991, Rutter *et al.* 1994).

Deformation experiments have been instrumental in describing characteristic microstructures, textures and constitutive equations (flow laws) associated with a variety of flow regimes. In turn, rock deformation experiments produce deformation microstructures and textures that may be compared with naturally deformed rocks. A comprehensive investigation by Schmid *et al.* (1987) illustrates the textures and microstructures in carbonates associated with a variety of deformation regimes. Rock deformation experiments are also used to define constitutive equations (flow laws) that relate strain rate to temperature, differential stress and grain size (e.g. Rutter 1974, Schmid 1982, Walker *et al.* 1990). However, several fabrics produced experimentally in marbles have not been observed in natural examples which suggests that some experiments do not duplicate natural conditions or that natural samples have not been studied from sufficiently varied environments.

Single-crystal calcite deformation experiments have defined specific slip and twin systems operative at different temperature, stress and strain rate conditions. Calcite deforms by twinning on *e* $\{\bar{1}018\}$ and *r* $\{10\bar{1}4\}$ (Turner *et al.* 1954) and slip on three dominant systems; *r* $\{10\bar{1}4\}$, *f* $\{\bar{1}012\}$, and *c* $\{0001\}$ (Turner *et al.* 1954, Turner & Orozco 1976, Spiers & Wenk 1980, De Bresser & Spiers 1993). Experiments define possible slip planes, directions and the critical resolved shear stresses

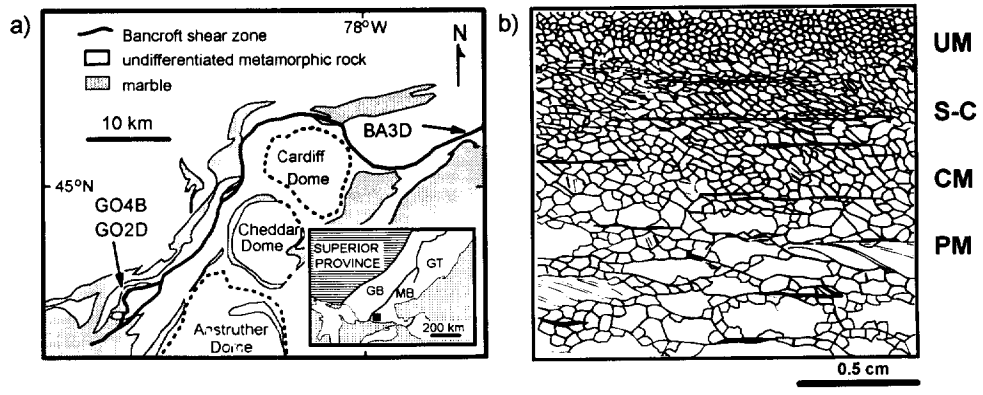

Fig. 1. (a) Location and generalized geologic map showing the outcrop trace of the Bancroft shear zone and locations of samples analyzed in this study. Inset shows major subdivisions of the Grenville province. Stipple pattern is Paleozic cover. Abbreviations are: GB = gneiss belt, MB = metasedimentary belt, GT = granulite terrane. (b) Sketch of microstructures in sample GO4B showing the transitions from protomylonite (PM) to coarse mylonite (CM) to *S–C* mylonite (*S–C*) to ultramylonite (UM). Absolute grain sizes are not true but the relative positions and microstructures are depicted as in thin section. Figures are modified from van der Pluijm (1991).

required for activity. This has allowed refinement of numerical models for geologic materials and the prediction of textures in rocks with a variety of strain histories and deformation conditions. Wenk *et al.* (1987) numerically predicted the fabrics that would be expected with differing slip system activity (a proxy for temperature) and strain paths. This numerical approach has produced a variety of theoretical textures, some of which mimic natural textures.

The experimental data, when applied to naturally deformed rocks, may yield information regarding deformation mechanisms, conditions of deformation (temperature, differential stress), and rates of tectonic processes. Naturally deformed calcite rocks studied thus far have had monotonous textures containing one maximum (Schmid *et al.* 1981, Dietrich & Song 1984, Heitzmann 1987, Wenk *et al.* 1987, Ratschbacher *et al.* 1991, Erskine *et al.* 1993). Generally these fabrics are consistent with low-temperature numerical models and experiments where **e** twinning and **r** slip were active. Random fabrics have only been reported by Schmid *et al.* (1981), Behrmann (1983) and Heitzmann (1987) which were attributed to grain-boundary sliding in fine grained (~10 μm) mylonites at elevated temperatures.

This paper presents results of a detailed investigation of microstructures and textures in calcite mylonites, which indicate that dislocation creep and grain-boundary sliding were important deformation mechanisms during mylonite development at relatively low temperatures. Some of the fabrics consistent with the 'high temperature' experiments and numerical models have not previously been found in naturally deformed rocks. The samples were collected from the Bancroft shear zone of the Grenville Orogen in Ontario, Canada, which preserves a complete sequence from undeformed marble protolith to ultramylonite (Carlson *et al.* 1990). Microstructures were previously described by van der Pluijm (1991); in this paper attention is given to textures. The primary goals of this study are to determine the mechanisms responsible for mylonite development and to assess factors controlling microstructural evolution. Application of experimentally-derived constitutive equations is then used to evaluate the rheological properties of marble mylonitization.

Detailed axial distribution analysis using photomosaics and an optical microscope equipped with a universal stage were used to determine relationships between microstructure (grain size and shape) and texture (crystallographic fabric) in several microstructural domains across a small-scale mylonite zone within the Bancroft shear zone. All domains except the protolith and finest ultramylonite occur within the same thin section (over a distance of 2 cm). Grain areas, long axes, short axes and long axis orientations were measured using photomosaics, a digitizing tablet and JANDEL software. A Leitz 4-axis universal stage was used for *c*-axis determinations. Cathodoluminescence microscopy was also used to assess secondary calcite growth features not visible with transmitted light microscopy. This description of texture and microstructure allows a direct comparison with experimentally produced textures and microstructures. It also provides a relational data base between crystallographic orientation and grain microstructure that would not be possible with bulk crystallographic fabric analysis (e.g. X-ray texture goniometry).

GEOLOGIC SETTING

The rocks analyzed in this study are from the Bancroft shear zone, which is located in the western Metasedimentary Belt of the southern Grenville Orogen (Fig. 1a) (Davidson 1986, Easton 1992). The zone is generally parallel to the regional thrust-related metamorphic foliation, which dips 30–40°SE. The Bancroft shear zone is a 15–20 m thick regionally extensive zone localized in marbles commonly occurring between more competent meta-igneous rock units. Typical outcrops expose branches of the shear zone 1–10 m thick in which abrupt transitions (<5 cm) from protolith to ultramylonite are

common. Field and microstructural sense-of-shear indicators suggest a normal shear sense for this SE-dipping shear zone (Carlson *et al.* 1990). The temperature of deformation was 450–500°C based on calcite–graphite C isotope thermometry (van der Pluijm & Carlson 1989, van der Pluijm 1991).

The transition from protolith to ultramylonite has been described as progressive mylonitization of light-colored, coarse grained marble, to dark grey well foliated and lineated mylonite (Carlson *et al.* 1990). A transition from protomylonite to ultramylonite is observed over the scale of a thin section (2 cm). The changes in texture and microstructure across this transition are the focus of this investigation. Figure 1(b) depicts the microstructural domains described below that are observed in the thin section. In addition, protolith and very fine ultramylonite samples were analyzed to characterize the complete range of textures and microstructures associated with the Bancroft shear zone.

MICROSTRUCTURES AND TEXTURES

Textural data complement microstructural observations and allow inference of the active deformation mechanisms by relating the data to experimental or numerical modelling results. Collectively, these data allow an assessment of the activity of specific slip systems, recrystallization mechanisms and other deformation mechanisms. The following microstructural descriptions will proceed from protolith to progressively deformed mylonites as indicated by increased fabric intensity (development of lineation and foliation) and particularly by progressive grain size reduction.

Protolith

The protolith is dominated by equant, coarse calcite grains with minor amounts of graphite, quartz, diopside and phlogopite (Figs. 2a and 4a). No dimensional preferred orientation (DPO) is evident (Fig. 4a) and only a weak color banding (grey–blue and white) defines the foliation in hand specimen. Grain boundaries are generally serrated, bulbous and interpenetrating. Grain interiors are dominated by twins. Commonly, twins narrow toward grain boundaries or are lensoid in shape, suggesting a mechanical origin and preservation of the host grain between lamellae. Undulose extinction and deformation bands are restricted to regions surrounding secondary phases (Figs. 2a and 4a). Recrystallization is evident only in a few places along grain boundaries and twin lamellae.

Crystallographic orientations of grains show no obvious preferred orientation (Fig. 4b). Poles of twin lamellae are consistently 26° from the host twin *c*-axis indicating twinning on *e* (Fig. 4c). Analysis of twin orientations by the method of Dietrich & Song (1984) indicates a compression direction consistent with the sense of shear inferred from other evidence (Fig. 4c). The *c*-axes of the small grains tend to be oriented at a high angle to the foliation while large grain *c*-axes are more dispersed (Figs. 4a & b).

Protomylonite and porphyroclastic mylonite

Protomylonite samples are composed of coarse calcite porphyroclasts surrounded by equant, smaller grains in a core and mantle microstructural geometry (Fig. 2b). A DPO is developed in porphyroclasts that are elongate and lie parallel or slightly oblique to the dominant foliation (shear plane, *C*). A weaker DPO is evident in the domains of recrystallized grains surrounding porphyroclasts (Figs. 2b & c). The aspect ratio decreases and the orientation of long axes are more dispersed in recrystallized matrix grains (Table 1). Grain boundaries of porphyroclasts are irregular with straight and curved segments while matrix grain boundaries are straight to slightly curved. The internal microstructures of porphyroclasts are characterized by undulatory extinction, deformation bands and subgrains. Matrix grains generally have sharp extinction with little subgrain development. Cathodoluminescence microscopy shows uniform luminescence in porphyroclasts while recrystallized matrix grains commonly have brightly luminescent rims (Figs. 3a & b).

Figures 5(a) & (b) show the relationship between microstructure and crystallographic orientation in a representative core and mantle structure. Subgrains in the porphyroclast are slightly misoriented (<10°) relative to one another, and the *c*-axis of adjacent recrystallized matrix grains have a great circle distribution. Large grain and porphyroclast *c*-axes in this domain tend to be oriented subperpendicular to the shear plane (maximum 1 in Fig. 6b), and matrix grain *c*-axes are distributed about a great circle containing the lineation (Figs. 6a & b). Two weak point maxima along the great circle girdle are inclined 20–30° from the shear plane (points 2 and 3 in Fig. 6b). A second porphyroclastic mylonite domain has a slightly larger grain size but similar microstructure and texture (Fig. 6c). The great circle girdle in this domain has a slightly different orientation than that previously described, perhaps reflecting a rotation of the local transport direction.

Coarse mylonite

Coarse mylonite domains consist entirely of dynamically recrystallized grains. The grain size and aspect ratio of these grains are essentially equal to the matrix grains in the protomylonite domain (Table 1). A weak DPO is illustrated by long axis orientations aligned oblique to the shear plane (Figs. 2d and 7a). Grains are characterized by sharp extinction and straight to slightly curved boundaries. Larger grains in this domain commonly have subgrain microstructure with subgrain sizes generally half the host grain size. Cathodoluminescence microscopy reveals many brightly luminescent rims of grains suggesting secondary overgrowth on most grains (Figs. 3c & d). Jagged 'extensional' seams, subparallel to

the shear plane, and fractures in secondary phases are filled with brightly luminescent secondary calcite as well (Figs. 3e & f). The texture of coarse mylonite is nearly random except for a lack of *c*-axes orientations in a band between the shear plane and the inferred flattening plane (Fig. 7b). Texture/microstructure relations indicate that large grains tend to have *c*-axes oriented at a high angle to the shear plane (Fig. 7a). Additionally, several groups of adjacent, similarly oriented grains are present, reflecting an inherited single grain orientation in these recrystallized grains.

S–C mylonite

Across an abrupt microstructural transition from mylonite to ultramylonite, grain size is reduced and a *S–C* fabric is developed, similar to those described in quartzites (Lister & Snoke 1980, Law *et al.* 1984, Burg 1986). Relative to adjacent domains the DPO is strong as indicated by alignment of long axes and greater aspect ratios (Table 1). Elongate grains aligned oblique (30°) to the shear plane define the *S*-foliation. Bands of finer, more elongate grains, mantled by very fine grained secondary phases, define the mesoscopic *C*-planes (Figs. 2e and 8a). The shear sense inferred from this microstructure is compatible with the compression direction inferred from twin analyses in the protolith (Fig. 4c) and mesoscopic shear sense indicators such as rotated clasts (Carlson *et al.* 1990). Grain boundaries are generally straight to curved, and internal microstructures are characterized by sharp extinction. However, subgrain development is common in larger grains (Fig. 8a). Cathodoluminescence is uniform.

The *c*-axis orientations show a preferential alignment perpendicular to the shear plane and a weak great circle girdle containing the lineation (Fig. 8b). Comparison of microstructure and *c*-axis orientation of grains in this domain shows that the most elongate grains tend to dominate the maximum perpendicular to the shear plane (Fig. 8a). The more equant grains that dominate the *S*-foliation lie throughout the great circle.

Ultramylonite

Decreased grain size and weakening of DPO characterize the transition from *S–C* mylonites to ultramylonite (Table 1). Two domains with 30±9 and 21±5 μm grain sizes were analyzed. Aspect ratios of grains in these domains decreases and alignment of grain long axes parallel to the shear plane increases with decreasing grain size (Table 1). Two populations of grains defined in the *S–C* mylonite are no longer present; rather, the microstructures are homogeneous and secondary phases are disseminated throughout the domain. Grain boundaries remain straight to curved in these finer domains (Figs. 2f, 9a & c). Grains generally have sharp extinction with subgrains developed in several grains. Cathodoluminescence is generally uniform with lightly contrasting bands parallel to the mylonitic flow banding.

Textures in ultramylonites are characterized by a strong point maximum subperpendicular to the shear plane and weak great circle girdles (Fig. 9b). In the finest ultramylonite domain this maximum is deflected in the shear direction toward the inferred extension direction (Fig. 9d). Comparison of microstructure and grain orientation shows an essentially random relationship except for occasional clustering of similarly oriented grains (Figs. 9a & c).

DISCUSSION

Deformation mechanisms

The dominant deformation mechanism may be inferred for each microstructural domain based on the observed microstructures and measured textures. Twin lamellae dominating the internal microstructure of protolith calcite grains provide evidence for twinning as the main crystal-plastic deformation mechanism. The lack of significant crystallographic preferred orientation (CPO) is attributed to low twin strains, which is supported by the preservation of host grains. Bulbous intergrowths and serrated grain boundaries suggest that some grain-boundary migration has occurred during deformation of the protolith. Fine grains are present along many grain boundaries and twin lamellae. Because large grains lack undulose extinction and a subgrain microstructure, and the grain boundaries are bulbous and interpenetrating, these fine grains are attributed to the activity of migration recrystallization (Urai *et al.* 1986). The *c*-axes of small grains tend to be oriented at a high angle to the macroscopic foliation (parallel to the shear zone) while most *c*-axes of large grains are more widely distributed (Figs. 4a & b). Based on the adjacent domainal fabrics, the large grains were unfavorably oriented for slip and have grown at the expense of favorably oriented grains via grain-boundary migration. This microstructure/texture relation is analogous to high strain-rate, low-temperature quartz deformation experiments by Gleason *et al.* (1993), which showed that migration recrystallization favored growth of grains unfavorably oriented for basal and prism slip. Protolith microstructures are genetically associated with mylonitization via the consistency of twin analyses in the protolith (Fig. 4c) and shear-sense indicators (Carlson *et al.* 1990).

Protomylonite and porphyroclastic mylonite samples are dominated by core and mantle structures. They experienced grain-size reduction via rotation recrystallization based upon progressive crystallographic mismatch of subgrains and new grains relative to the core of porphyroclasts (Fig. 5). Undulatory extinction, deformation bands, and subgrains suggest that dislocation creep was the dominant deformation mechanism, which is supported by the development of a CPO associated with this microstructure (Figs. 6b & c). In addition, the presence of secondary overgrowths on many grains suggests solution mass transfer was also active (Fig. 3b). Comparison of this texture with those produced experi-

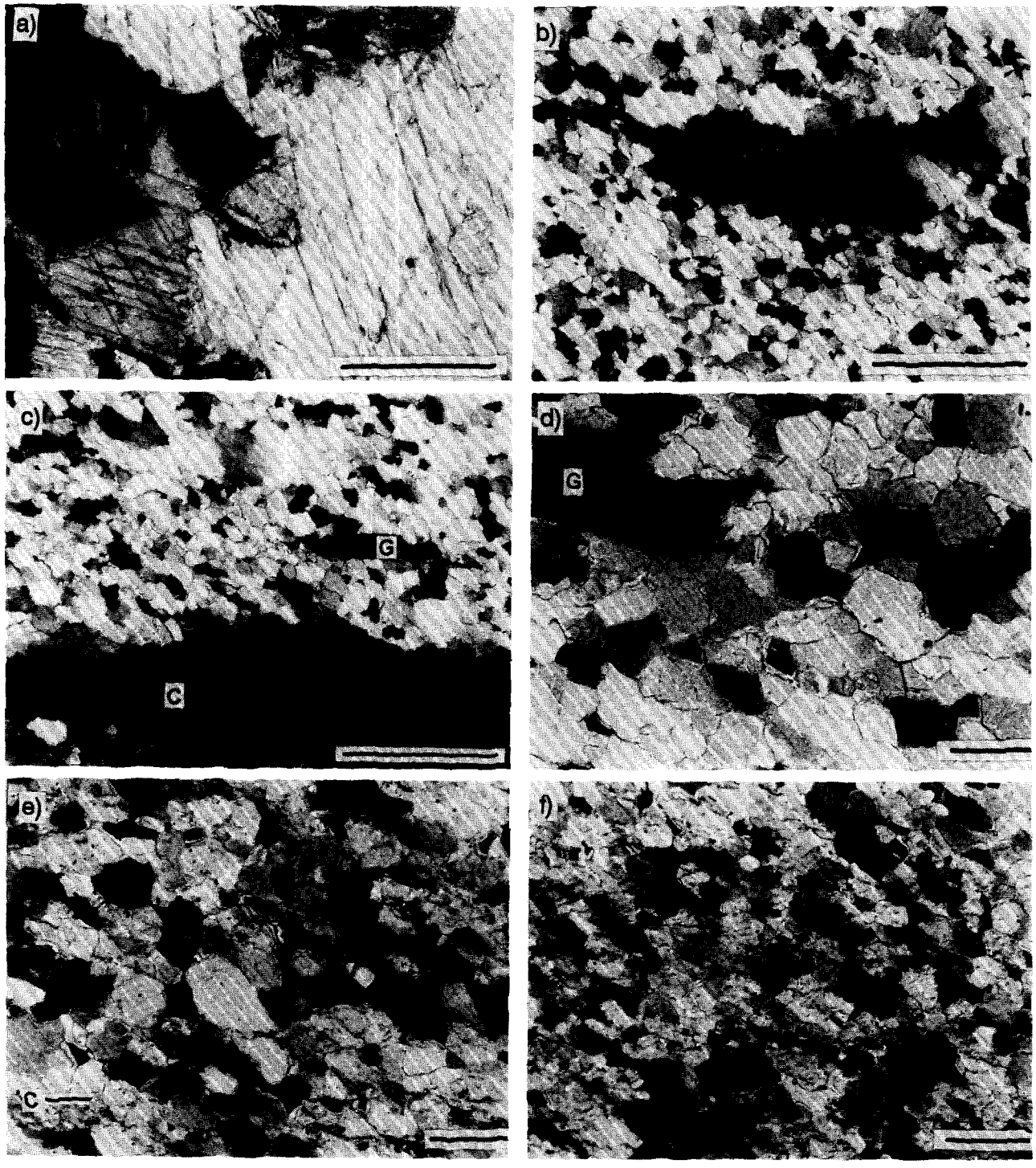

Fig. 2. Photomicrographs of textural domains taken with crossed nicols. Scale bars for (a), (b) & (c) are 500 μm and for (d), (e) & (f) 100 μm. (a) Protolith showing mechanical twins, serrated grain boundaries, and undulose extinction near secondary phases (sample GO2D). (b) Porphyroclast with undulose extinction, subgrain development and surrounding dynamically recrystallized matrix grains (sample GO4B). (c) Porphyroclastic mylonite showing fine-grained, equigranular matrix surrounding a porphyroclast (C) and graphite grain (G) (sample GO4B). (d) Coarse mylonite with equigranular texture and coarse secondary phase (graphite, G) (sample GO4B). (e) *S–C* mylonite with well developed dimensional preferred orientation and bands of finer grains with disseminated secondary phases defining *C*-domains (sample GO4B). (f) Fine ultramylonite with secondary phases disseminated throughout the domain and a moderately well developed DPO (sample GO4B).

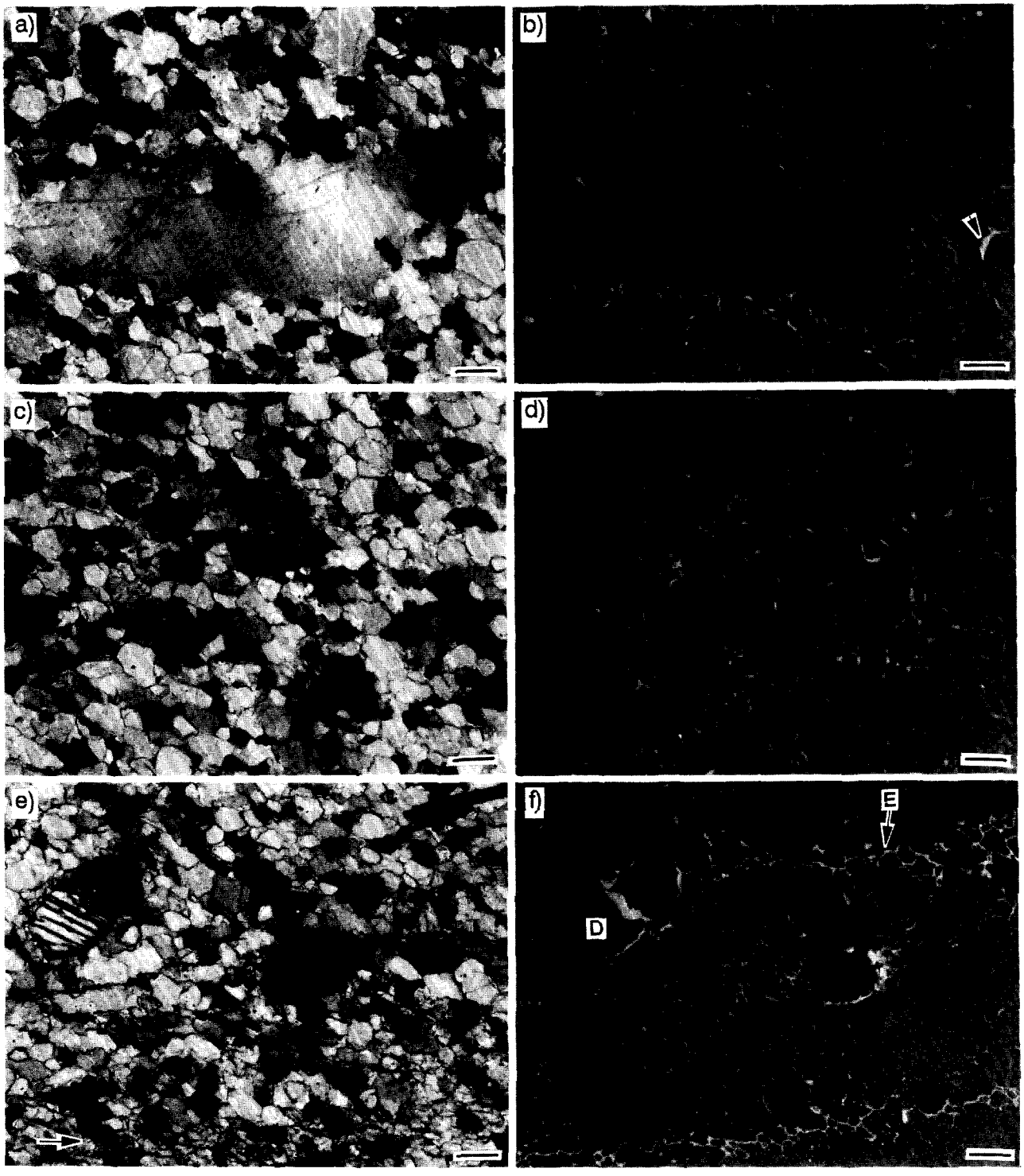

Fig. 3. (a) Photomicrograph of porphyroclastic mylonite (same grain as Figs. 2b and 5) taken with crossed nicols. (b) Cathodoluminescence photomicrograph of same area as (a) showing brightly luminescent rims along many recrystallized matrix grains (arrow). (c) Photomicrograph of coarse mylonite taken with crossed nicols. (d) Cathodoluminescence photomicrograph of same area as (c) showing brightly luminescent rims along many grains suggesting secondary calcite growth. (e) Photomicrograph of coarse mylonite near the transition to *S–C* mylonite (arrow) taken with crossed nicols. (f) Cathodoluminescence photomicrograph of same area as (e) showing brightly luminescent rims on many grains, fractured diopside grain (D) with secondary calcite filling the fracture, and extensional seams (E) which follow grain boundaries filled with secondary calcite. These photographs indicate solution mass transfer in the coarse mylonite and matrix of protomylonite domains. Cathodoluminescence operating conditions were 6 μA and 12 kV. Scale bars are 100 μm.

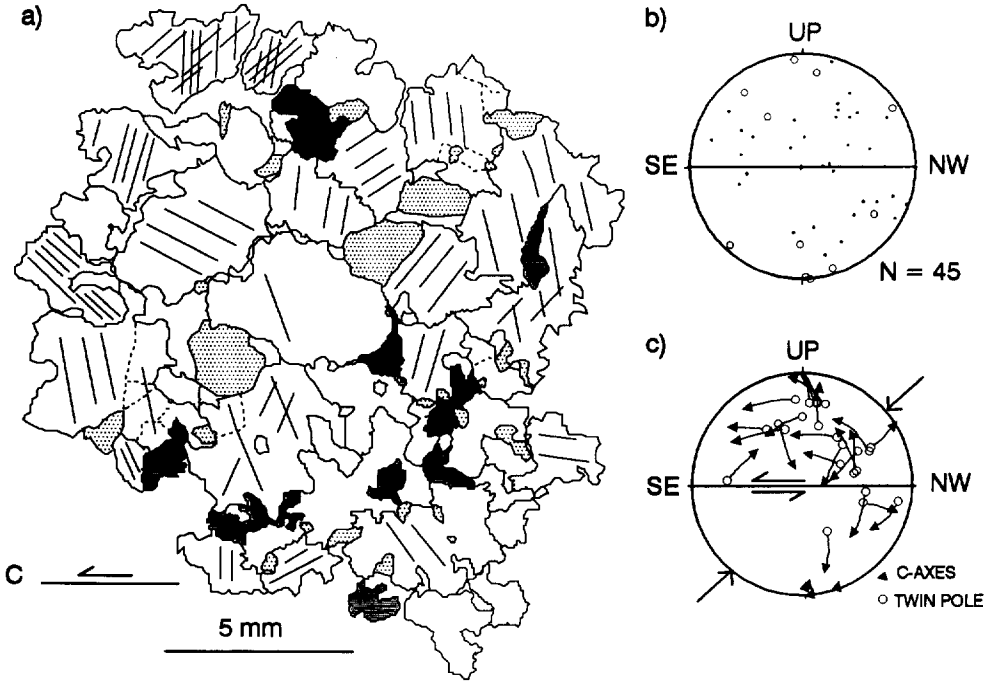

Fig. 4. (a) Line tracing of photomosaic of protolith sample (GO2D) showing bulbous, serrated, interpenetrating grain boundaries. Light stippled areas are secondary phases. Dark stippled areas are small grains plotted in open circles in (b). Dashed lines are subgrain boundaries. Solid straight lines are twin lamellae. (b) Equal area lower hemisphere projection of *c*-axes. Open circles correspond to small grain [dark stipple in (a)] orientations. (c) Twin analysis method of Dietrich & Song (1984) indicating a compression direction consistent with top to the southeast sense of shear.

Table 1. Textural characteristics of marble mylonites. Numerical values are mean (standard deviation)

Domain	Grain size (μm)	Aspect ratio	Long axis orientation*
Protolith n = 45 GO2D	1600 (800)	1.76 (0.54)	−10 (51)
Porphyroclasts n = 20	115 (29)	2.06 (0.67)	29 (24)
Matrix n = 280 GO4B	47 (16)	1.64 (0.50)	23(46)
Porphyroclasts n = 20	229 (78)	2.46(0.93)	12(13)
Matrix n = 253 GO4B	67 (29)	1.67 (0.50)	20 (39)
Coarse mylonite n = 443 GO4B	51 (18)	1.68 (0.46)	39 (40)
S–C mylonite n = 222 GO4B	38 (13)	1.96 (0.55)	28 (22)
Ultra-mylonite n = 272 GO4B	30 (9)	1.83 (0.47)	30 (25)
Fine ultra-mylonite n = 191 BA3D	21 (5)	1.75 (0.49)	−5 (26)

*Measured clockwise from shear plane.

mentally in the intracrystalline slip regime by Schmid *et al.* (1987) suggests that slip occurred on *r*, *f* and *c* slip systems, because the textures contain point maxima distributed about the primitive circle in a similar geometric relationship (points, 1, 2 and 3 in Fig. 6b). Preference of large grains to be oriented in near maximum 1 suggests that rotation recrystallization changes the texture from a single point maximum to a more distributed great circle girdle. The texture of the second porphyroclastic mylonite domain (Fig. 6c) is slightly misoriented (by 20–30°) relative to the other domain which suggests flow lines varied over small distances (1 cm).

Coarse mylonite, consisting entirely of recrystallized grains with shape and size comparable to recrystallized matrix grains in porphyroclastic mylonite, has a nearly random texture (Table 1 and Fig. 7b). Random textures cannot be produced by twinning or dislocation creep and rotation recrystallization, which are the dominant mechanisms in surrounding domains. A possible mechanism that randomizes textures is grain-boundary sliding (GBS). Pressure-sensitive GBS is not likely at these conditions and there is no microstructural evidence of cataclasis. The dominant deformation mechanism in this domain is diffusion- or dislocation-controlled GBS (typically associated with superplasticity) (e.g. Pilling 1989), however, the coarse grain size (50 μm) associated with domain is not consistent with much previous work where grain-boundary sliding was inferred (Behrmann 1983, Schmid *et al.* 1981, 1988, Heitzmann 1987). The extent to which grain growth has altered the coarse mylonite grain size cannot be evaluated, but the preservation of deformation microstructures throughout the sample suggests grain growth due to annealing was minimal.

Fluid likely influenced deformation in the coarse

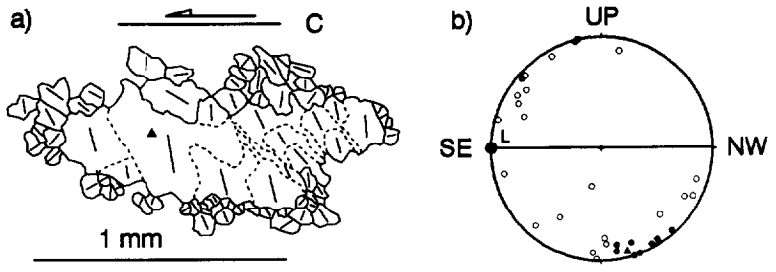

Fig. 5. (a) Line tracing of calcite porphyroclast with subgrains surrounded by new grains (sample GO4B). The triangle indicates the 'core' grain. Straight lines in grain interiors are projections of *c*-axes. (b) Crystallographic orientations of core (triangle), subgrains (solid circles), and new grains (open circles).

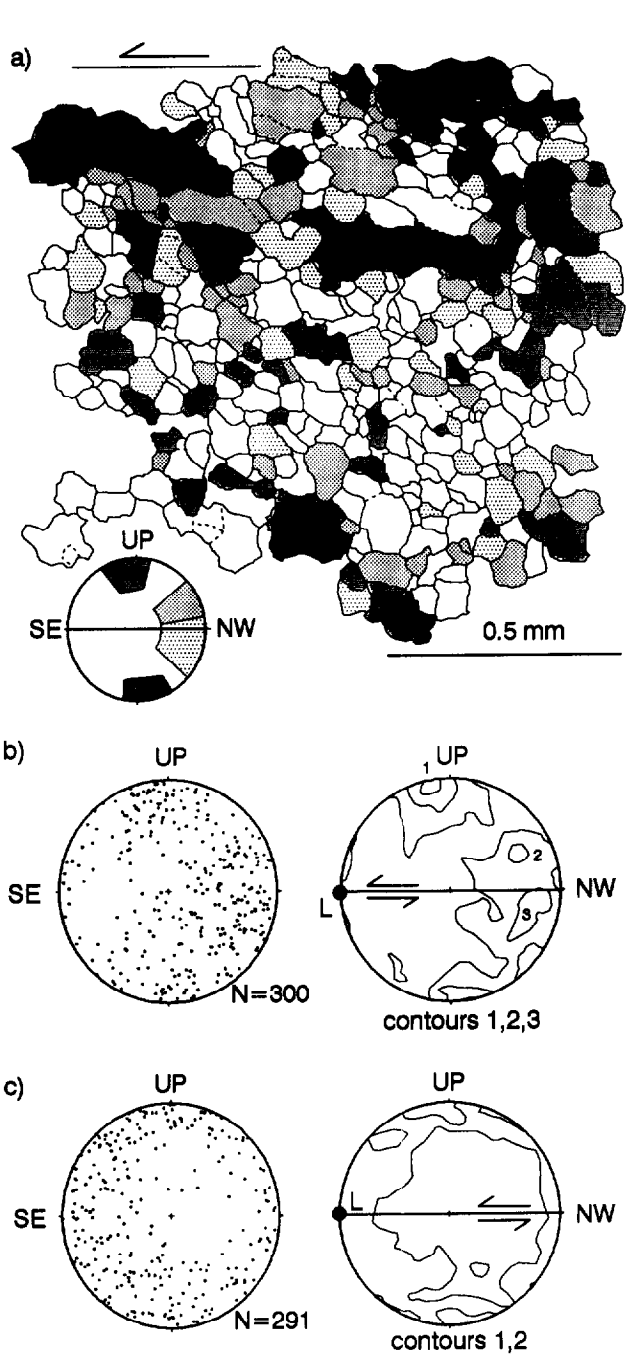

Fig. 6. (a) Line tracing of porphyroclastic mylonite (sample GO4B). Shaded grains in line tracings have *c*-axis orientations that lie in the similarly shaded area of the corresponding stereonet. (b) Equal area lower hemisphere projection of *c*-axes orientations of grains in (a). Contours are multiples of a uniform distribution in contoured plots. (c) Orientations of *c*-axes in another porphyroclastic mylonite domain.

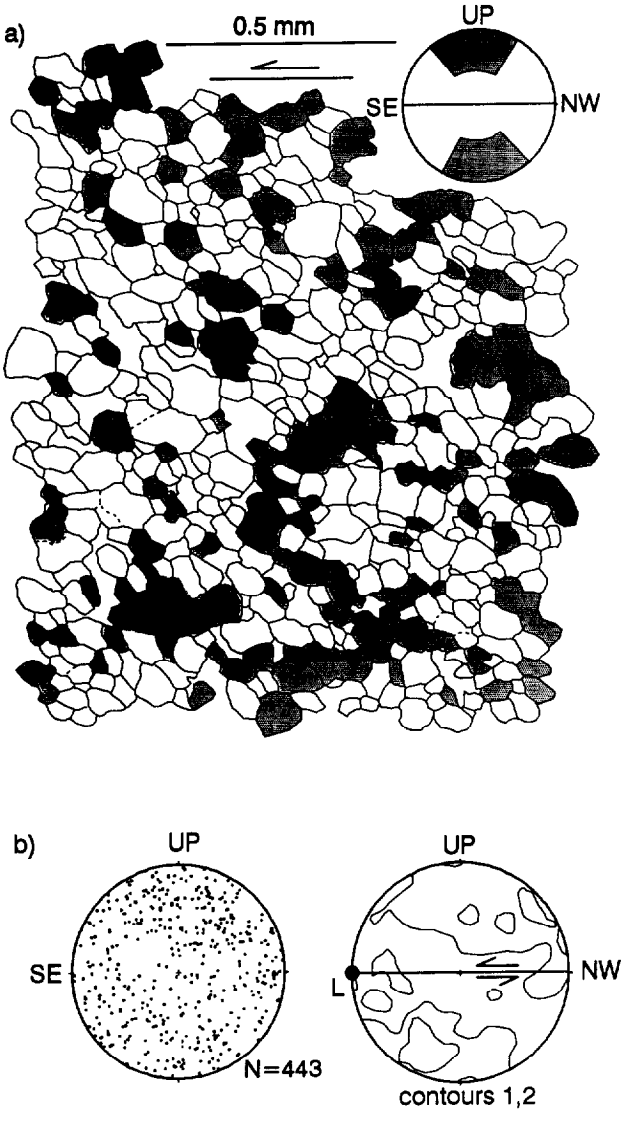

Fig. 7. (a) Line tracing of coarse mylonite (sample GO4B). (b) Orientations of *c*-axes of grains in (a). See Fig. 6 for further explanation.

mylonite. Cathodoluminescence microscopic observations of secondary overgrowths on rims of grains in the matrix of the porphyroclastic mylonite and coarse mylonite domains, and fractures filled with secondary calcite suggest that dissolution and new growth occurred (Fig. 3). Carlson (1988) and van der Pluijm & Carlson (1989) presented oxygen isotope data for these mylonites that show a change in $\delta^{18}O$ from 26‰ in the protolith to 16‰

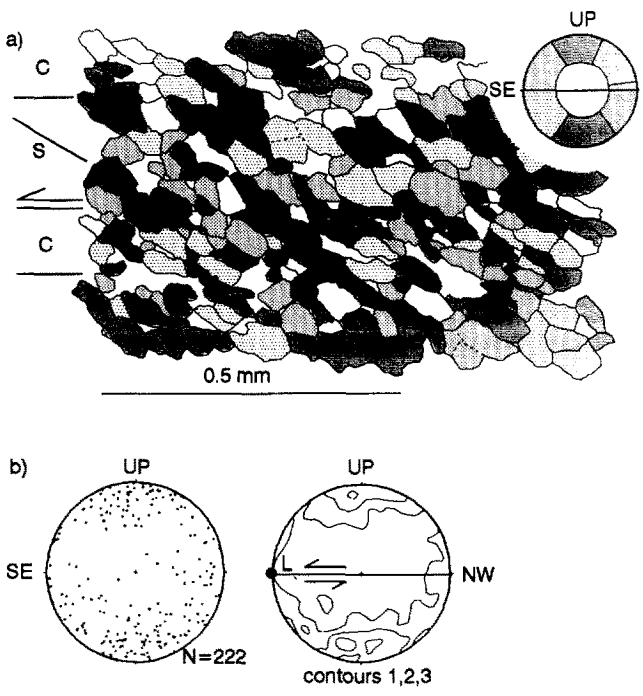

Fig. 8. (a) Line tracing of *S–C* mylonite (sample GO4B). (b) Orientations of *c*-axes of grains in (a). Horizontal lines on the left define *S* and *C* domains. See Fig. 6 for further explanation.

in the ultramylonites. These dramatic changes occur on scales down to thin sections. A simple calculation using the formulation of Taylor (1977) relates this 10‰ change to a fluid to rock ratio of 2:1 to 7:1 for open or closed systems, respectively, given a reasonable initial fluid composition for the regional lithology (orthogneisses; 10–12‰, Taylor 1974). This large flux of fluid enhanced grain-boundary diffusion and dissolution. Grain-boundary sliding was aided by dissolution at high-stress grain contacts. This dissolution is balanced by local precipitation, which in turn may become dissolution sites as the microstructure evolves. As a consequence of such transient grain boundaries, relatively large grains were able to easily slide past one another and rotate by this mechanism of fluid-assisted GBS.

The presence of a weak fabric in coarse mylonite, illustrated by the lack of orientations along a band between the inferred flattening plane and shear plane, and preferred orientation of large grains (Fig. 7a), suggests that dislocation creep was active to some extent. This domain may be analogous to the transitional regime of Walker *et al.* (1990) and Rutter *et al.* (1994), which was characterized by contributions of GBS and dislocation creep in deformation of calcite rocks with grain sizes up to 40 μm.

Fine mylonites (*S–C*, ultramylonite) have a well defined CPO and well to moderately developed DPO. The CPO and DPO are attributed to dislocation creep. The decreased grain sizes in these domains is attributed to rotation recrystallization as indicated by some subgrain development. Strengthening of the point maximum (Figs. 8b and 9b) may represent an 'easy slip' orientation for glide on *c* possibly assisted by grain-boundary migration (Schmid & Casey 1986, Schmid *et al.* 1987). Knipe and Law (1987) found that grain-boundary migration leads to a grain-size distribution across girdled quartz fabrics. Grain-boundary migration may not be as significant here because there is no obvious grain-size distribution. Elongate grains, both large and small, enhance the maximum (Fig. 8a). Additionally, these elongate grains dominate the *C*-domains (Figs. 2e and 8a) which are likely domains of higher strain and have grain boundaries pinned by secondary phases (Ratschbacher & Neubauer 1989, Olgaard 1990, Walker *et al.* 1990). This implies that increased strain promotes the 'easy slip' orientation possibly until the elongate grain recrystallizes and changes orientation. The most evolved ultramylonite has a fabric which suggests that at high strains the maximum rotates toward the extension direction. If this maximum is associated with *c*-slip, the crystallographic slip-plane rotates through the shear plane.

The varied deformation mechanisms that operated simultaneously and over short distances within the shear zone have important implications for the interpretation of deformation mechanisms from microstructures alone. One would expect dislocation creep associated fabrics from core and mantle structures and dynamically recrystallized grains such as the protomylonite and porphyroclastic mylonite presented here. However, in the coarse mylonite domain the fabric data clearly show that another mechanism (GBS) was dominant. Comparison with much of the published data on GBS would suggest that the coarse mylonite grain size is too large for GBS activity. However, recent experimental results of Walker *et al.* (1990) lend support for GBS activity in relatively coarse grains (2–40 μm). One may expect GBS to have been operative in the finest mylonite domains studied here (van der Pluijm 1991), but the fine mylonites have well developed CPOs attributed to dislocation creep. The absence of a random fabric is likely explained by dissemination of secondary phases in fine mylonites, which inhibit grain-boundary motion thereby favoring dislocation creep.

The variety of deformation mechanisms interpreted here are generally not found in experiments performed under similar conditions. The importance of secondary phases, strain magnitude, and microstructural parameters (grain size and shape) is significant so that strict application of experimental results may often not be warranted (e.g. Paterson 1987). Protomylonite, coarse mylonite, and *S–C* mylonite contain inhomogeneous texture/microstructure relations that are a function of the degree of mylonitization which is strain (time) dependent. Therefore, these are likely non-steady state textures and microstructures. In contrast, the fine ultramylonites have homogeneous microstructures with dissemination of all secondary phases and thus are more likely representative of steady-state flow. Thus these domains are most appropriate for extrapolation of

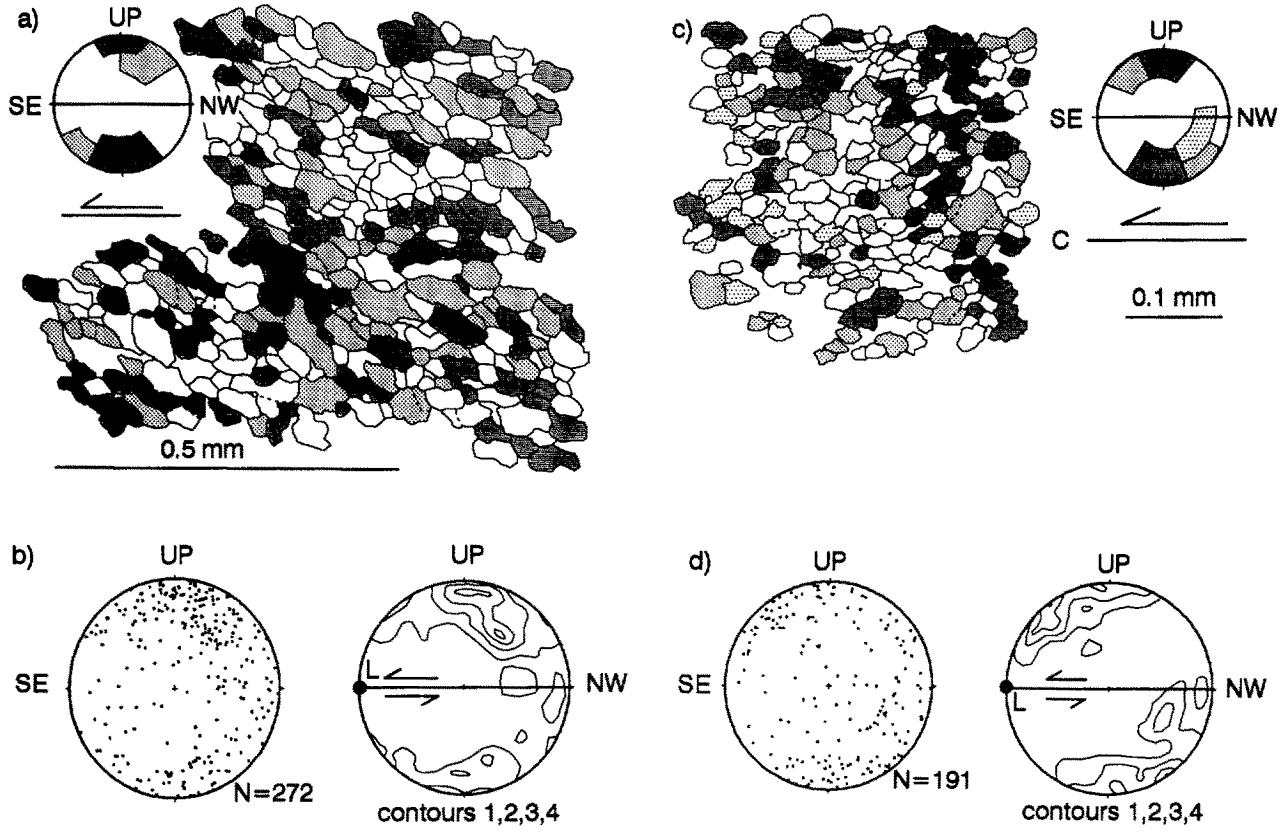

Fig. 9. (a) Line tracing of ultramylonite (sample GO4B). (b) Orientations of *c*-axes of grains in (a). (c) Line tracing of fine ultramylonite (sample BA3D). (d) Orientations of *c*-axes of grain in (d). See Fig. 6 for further explanation.

experimentally determined constitutive flow laws to determine quantitative rheological properties. Nonetheless, the transitions in deformation mechanisms have important implications for rheology and mylonite development.

Mylonite development and flow

The varied deformation processes interpreted from microstructure and textures imply significant differences in rheological properties across the transitions from protolith to ultramylonite. The temporal microstructural evolution of these mylonites can be described if it is assumed that ultramylonite domains were previously composed of coarser grains with microstructures and textures similar to those toward the margin of the shear zone. The transition from protomylonite to ultramylonite can be observed over a distance of 2 cm in a single thin section. Several microstructural observations indicate that the temporal evolution of mylonites may be represented by the fabric transitions across the shear zone. Large twinned grains in the protomylonite have microstructures similar to the protolith marble, although the grains have curved and bent twins and undulose extinction. Matrix grains in the porphyroclastic mylonite have microstructural characteristics nearly identical to the coarse mylonite, which is inferred to be the next stage in the temporal sequence. In addition, the transitions in graphite microstructures from euhedral flakes to strung-out, segmented trains to microscopic, graphite-rich bands, to homogeneously distributed graphite in ultramylonites tracks the progressive deformation of this phase in the shear zone (van der Pluijm 1991). Although one cannot be certain that the finest ultramylonite passed through all the stages represented by the other fabric domains, the preservation of some microstructural characteristics across the microstructural transitions is suggestive of a temporal sequence.

Constitutive equations from Rutter (1974), Schmid (1982), and Walker *et al.* (1990) were used to construct a deformation regime map that shows how stress varies as a function of grain size at constant temperature (Table 2). These equations were chosen by comparing the microstructures, textures and inferred deformation mechanisms of experimental material with those of our natural example. Rutter (1974) developed exponential flow laws for coarse grained Carrara marble which has grain size and microstructure similar to the protolith. Walker *et al.* (1990) conducted a series of experiments on synthetic calcite rocks with grain sizes, microstructure, and inferred deformation mechanisms similar to the coarse- and fine-grained mylonites in this study. Applying the constitutive equations generated during these experiments will allow inferences to be made regarding the rheology and conditions of flow during mylonite development.

During the onset of shear zone deformation the coarse grained protolith underwent low strains (based on preservation of host grains) due to twinning. This stage of mylonite development is represented by point A in Fig.

Table 2. Experimentally derived constitutive equations used to construct deformation regime map

Power law creep $\log \dot{e} = -5.5 - 314\text{kJ}/2.303RT + 6.0 \log \sigma$	Schmid (1982)
Exponential law creep $\log \dot{e} = 5.77 - 260\text{kJ}/2.303RT + 0.038\,\sigma$	Rutter (1974)
Grain-size sensitive creep $\log \dot{e} = 2.00 - 190\text{kJ}/2.303RT + 3.33 \log \sigma - 1.34 \log d$	Walker *et al.* (1990)
$\log \dot{e} = 4.93 - 190\text{kJ}/2.303RT + 1.67 \log \sigma - 1.87 \log d$	Walker *et al.* (1990)
Stress vs. recrystallized grain size $\log \sigma = 3.67 - 1.01 \log d$	Schmid *et al.* (1977)

$\dot{e}$ = strain rate (s^{-1}).
σ = differential stress (MPa).
T = absolute temperature (K).
R = gas constant (0.008314kJ/mol K).
d = grain size (μm).

10. Point A is located at the protolith grain size and minimum stress required to place the point in the exponential creep (twinning) regime. Strain rate is relatively fast but was likely short lived as indicated by the low finite strains inferred in the protolith. Dislocation creep subsequently dominates deformation either because twinning cannot keep pace with the imposed strain rate and/or strain becomes more localized.

The activity of dislocation creep produced a subgrain microstructure representative of rotation recrystallization. Core and mantle structures developed and the texture became dominated by a great circle distribution. The progression from protolith to protomylonite due to dislocation creep and rotation recrystallization is represented by the path from point A to B (Fig. 10). This deformation regime is the dislocation creep regime of Walker *et al.* (1990), characterized by shape fabric and texture development and a minor GBS component. The location of point B on the map is constrained by the grain size of porphyroclasts and stress inferred from the recrystallized grain size/stress relation of Schmid *et al.* (1980). Subsequently, equant, smaller grains (region C) produced by rotation recrystallization dominate the microstructure. Flow during this stage of mylonite development is characterized by strain softening. Conditions of constant stress and increased strain rate or stress drop characterize flow. Region C is associated with the coarse mylonite and lies in the GBS-dominated regime. A transition from dislocation creep to GBS may be expected with an increase in temperature or decrease in grain size. Because grain size is decreasing and previous work (van der Pluijm & Carlson 1989, van der Pluijm 1991) indicates constant or decreasing temperature, these relations indicate that GBS was initiated by microstructural changes (grain size and shape) due to rotation recrystallization and strain softening results.

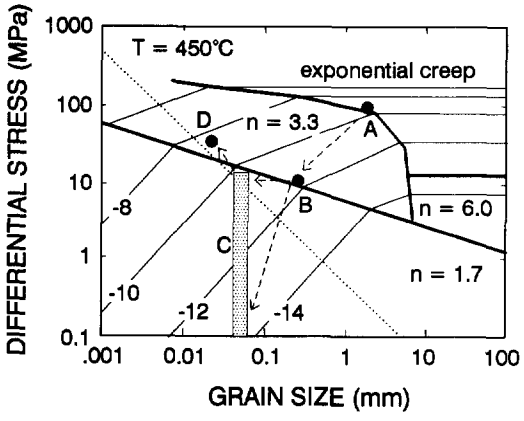

Fig. 10. Deformation regime map constructed using constitutive equations from Walker *et al.* (1990) for regimes $n = 1.7$ and $n = 3.3$, Schmid (1982) for regime $n = 6.0$, and Rutter (1974) for exponential creep (Table 2). Map was constructed for $T = 450$°C. Contours are log strain rate. Points A–D represent deformation regimes for domains studied. Dotted line is the recrystallized grain size stress relation from Schmid *et al.* (1980). Heavy lines separate regimes with different dominant deformation mechanism.

In finer grained ultramylonites CPOs are developed and DPOs are strengthened. Deformation in this domain is represented by point D (Fig. 10). Point D is constrained by a grain size that must lie in the dislocation creep-dominated field. This position is only attainable with a rise in stress as grain size decreases (path C–D). Therefore, the transition from GBS-dominated flow to dislocation creep is characterized by work hardening. The microstructural parameter that affected this unusual transition is the disseminated secondary phases in *S–C* and ultramylonitic domains. The effect of secondary phases is to pin grain boundaries, making them less mobile, thereby hindering GBS. Addition of a secondary phase (alumina) in samples deformed by Walker *et al.* (1990) was found to inhibit grain growth and increase strength (hardening), which lends support to this interpretation.

The microstructures described here indicate a complex interplay between strain rate, stress, microstructure and secondary phases. Many deformation mechanisms operated simultaneously within the same domain and over small distances. The competition between deformation mechanisms was highly sensitive to the conditions of deformation. These conditions not only included temperature, differential stress and strain rate, but strain, grain size and distribution of secondary phases (solids and fluids) as well.

Acknowledgements—Research was supported by the National Science Foundation (grant EAR93-05736), Geological Society of America Research Grant, the Scott Turner Fund of the Department of Geologi-

cal Sciences. We thank Eric Essene for careful reviews of this manuscript, and Bernard Housen, Stephen Kesler, Charlie Onasch and Stephen Potts for helpful discussions. Thanks to Journal referees L. Ratschbacher and E.H. Rutter and editor S.F. Wojtal for comments and suggestions that improved the manuscript. Tracy Frank is thanked for her assistance with cathodoluminescence microscopy.

REFERENCES

Behrmann, J. H. 1983. Microstructure and fabric transitions in calcite tectonites from the Sierra Alhamilla (Spain). *Geol. Rdsch.* **78**, 605–618.

Burg, J. P. 1986. Quartz shape fabric variations and *c*-axis fabrics in a ribbon-mylonite: arguments for an oscillating foliation. *J. Struct. Geol.* **8**, 123–131.

Carlson, K. A. 1988. Marble mylonites of the Bancroft shear zone, Ontario Grenville. Unpublished M.Sc. thesis. University of Michigan, Ann Arbor, Michigan.

Carlson, K. A., van der Pluijm, B. A. & Hanmer, S. 1990. Marble mylonites of the Bancroft shear zone: Evidence for extension in the Canadian Grenville. *Bull. geol. Soc. Am.* **102**, 174–181.

Davidson, A. 1986. New interpretations in the southwestern Grenville Province. In: *The Grenville Province* (edited by Moore, J. M., Davidson, A. & Bauer, A. J.). *Spec. Pap. geol. Ass. Can.* **31**, 61–74.

De Bresser, J. H. P. & Spiers, C. J. 1993. Slip systems in calcite single crystals deformed at 300–800°C. *J. geophy. Res.* **98**, 6397–6409.

Dietrich, D. & Song, H. 1984. Calcite fabrics in a natural shear environment, the Helvetic nappes of western Switzerland. *J. Struct. Geol.* **6**, 19–32.

Easton, R. M. 1992. The Grenville Province and the Proterozoic history of central and southern Ontario. In: *Geology of Ontario* (edited by Thurston, P. C., Williams, H. R., Sutcliffe, R. H. & Stott, G. M.). *Geol. Surv. Ontario* **4**, 715–904.

Erskine, B. G., Heidelbach, F. & Wenk, H.-R. 1993. Lattice preferred orientations and microstructures of deformed Cordilleran marbles: correlation of shear indicators and determination of strain path. *J. Struct. Geol.* **15**, 1189–1205.

Friedman, M. & Higgs, N. G. 1976. Calcite fabrics in experimental shear zones. In: *Mechanical Behavior of Crustal Rocks—The Handin Volume* (edited by Carter, N. L., Friedman, M., Logan, J. M. & Stearns, D. W.). *Am. Geophys. Un. Geophys. Monogr.* **24**, 11–27.

Gleason, G. C., Tullis, J. & Heidelbach, F. 1993. The role of dynamic recrystallization in the development of lattice preferred orientation in experimentally deformed quartz aggregates. *J. Struct. Geol.* **15**, 1145–1168.

Goetze, C. & Kohlstedt, D. L. 1977. The dislocation structure of experimentally deformed marble. *Contrib. Mineral. Petrol.* **59**, 293–306.

Groshong, R. H., Teufel, L. W. & Gasteiger, C. 1984. Precision and accuracy of the calcite strain-gauge technique. *Bull. geol. Soc. Am.* **95**, 357–363.

Heitzmann, P. 1987. Calcite mylonites in the Central Alpine "root zone". *Tectonophysics* **135**, 207–215.

Kern, H. & Wenk, H.-R. 1983. Calcite texture development in experimentally induced ductile shear zones. *Contrib. Mineral. Petrol.* **83**, 231–236.

Knipe, R. J. & Law, R. D. 1987. The influence of crystallographic orientation and grain-boundary migration on microstructural and textural evolution in an *S–C* mylonite. *Tectonophysics* **135**, 155–169.

Law, R. D., Knipe, R. J. & Dayan, H. 1984. Strain path partitioning within thrust sheets: microstructural and petrofabric evidence from the Moine Thrust zone at Loch Eriboll, northwest Scotland. *J. Struct. Geol.* **6**, 477–497.

Lister, G. S. & Snoke, A. W. 1980. *S–C* mylonites. *J. Struct. Geol.* **6**, 617–638.

Olgaard, D. L. 1990. The role of second phase in localizing deformation. In: *Deformation Mechanisms, Rheology and Tectonics* (edited by Knipe, R. J. & Rutter, E. H.). *Spec. Publ. geol. Soc.* **54**, 175–181.

Paterson, M. S. 1987. Problems in the extrapolation of laboratory rheological data. *Tectonophysics* **133**, 33–43.

Pilling, J. 1989. *Superplasticity in Crystalline Solids*. Institute of Metals, London.

Ratschbacher, L. & Neubauer, F. 1989. West-directed décollement of Austro-Alpine cover nappes in the eastern Alps: geometrical and rheological considerations. In: *Alpine Tectonics* (edited by Coward, M. P., Dietrich, D. & Park, R. G.). *Spec. Publ. geol. Soc.* **45**, 243–262.

Ratschbacher, L., Wenk, H.-R. & Sintubin, M. 1991. Calcite textures: examples from nappes with strain-path partitioning. *J. Struct. Geol.* **13**, 369–384.

Rutter, E. H. 1974. The influence of temperature, strain rate and interstitial water in the experimental deformation of calcite rocks. *Tectonophysics* **22**, 311–334.

Rutter, E. H., Casey, M. & Burlini, L. 1994. Preferred crystallographic orientation development during plastic and superplastic flow of calcite rocks. *J. Struct. Geol.* **16**, 1431–1446.

Schmid, S. M. 1982. Laboratory experiments on rheology and deformation mechanisms in calcite and their application to studies in the field. *Mitt. geol. Inst. ETH Univ. Zurich* **241**, 1–105.

Schmid, S. M., Boland, J. N. & Paterson, M. S. 1977. Superplastic flow in finegrained limestone. *Tectonophysics* **43**, 257–291.

Schmid, S. M. & Casey, M. 1986. Complete fabric analysis of some commonly observed quartz *c*-axis patterns. *Am. Geophys. Un., Geophys. Monogr.* **36**, 203–268.

Schmid, S. M., Casey, M. & Starkey, J. 1981. The microfabric of calcite tectonites from the Helvetic nappes (Swiss Alps). In: *Thrust and Nappe Tectonics* (edited by McClay, K. R. & Price, N. J.). *Spec. Publ. geol. Soc. Lond.* **9**, 151–158.

Schmid, S. M., Panozzo, R. & Bauer, S. 1987. Simple shear experiments on calcite rocks: rheology and microfabric. *J. Struct. Geol.* **9**, 747–778.

Schmid, S. M., Paterson, M. S. & Boland, J. N. 1980. High temperature flow and dynamic recrystallization in Carrara marble. *Tectonophysics* **65**, 245–280.

Spiers, C. J. & Wenk, H.-R. 1980. Evidence for slip on *r* and *f* in the positive sense in deformed calcite single crystals. *EOS Trans. AGU* **61**, 1128.

Taylor, H. P. Jr. 1974. The application of oxygen and hydrogen isotope studies to problems of hydrothermal alteration and ore deposition. *Econ. Geol.* **69**, 843–883.

Taylor, H. P. Jr. 1977. Water/rock interactions and the origin of H_2O in granitic batholiths. *J. geol. Soc. Lond.* **133**, 509–558.

Turner, F. J., Griggs, D. T. & Heard, H. 1954. Experimental deformation of calcite crystals. *Bull. geol. Soc. Am.* **65**, 883–934.

Turner, F. J. & Orozco, M. 1976. Crystal bending in metamorphic calcite, and its relation to associated twinning. *Contrib. Mineral. Petrol.* **57**, 83–97.

Turner, F. J. & Weiss, L. E. 1963. *Structural Analysis of Metamorphic Tectonites*. McGraw-Hill, New York.

Urai, J. L., Means, W. D. & Lister, G. S. 1986. Dynamic recrystallization of minerals. In: *Mineral and Rock Deformation: Laboratory Studies—The Paterson Volume* (edited by Hobbs, B. E. & Heard, H. C.). *Am. Geophys. Un. Geophys. Monogr.* **36**, 247–261.

van der Pluijm, B. A. 1991. Marble mylonites in the Bancroft shear zone, Ontario, Canada: microstructures and deformation mechanisms. *J. Struct. Geol.* **13**, 1125–1135.

van der Pluijm, B. A. & Carlson, K. A. 1989. Extension in the Central Metasedimentary Belt of the Ontario Grenville: timing and tectonic significance. *Geology* **17**, 161–164.

Wagner, F., Wenk, H.-R., Kern, H., Van Houtte, P. & Esling, C. 1982. Development of preferred orientation in plane strain deformed limestone: experiment and theory. *Contrib. Mineral. Petrol.* **80**, 132–139.

Walker, A. N., Rutter, E. H. & Brodie, K. H. 1990. Experimental study of grain-size sensitive flow of synthetic, hot-pressed calcite rocks. In: *Deformation Mechanisms, Rheology and Tectonics* (edited by Knipe, R. J. & Rutter, E. H.). *Spec. Publ. geol. Soc.* **54**, 259–284.

Wenk, H.-R., Takeshita, T., Bechler, E., Erskine, B. G. & Matthies, S. 1988. Pure shear and simple shear calcite textures: comparison of experimental, theoretical and natural data. *J. Struct. Geol.* **9**, 731–745.

Wenk, H.-R., Takeshita, T., Van Houtte, P. & Wagner, F. 1986. Plastic anisotropy and texture development in calcite polycrystals. *J. geophys. Res.* **91**, 3861–3869.